American Mineralogist, Volume 77, pages 359–373, 1992

Microstructures in natural perovskites

MEISHENG HU,* HANS-RUDOLF WENK, DARIA SINITSYNA**
Department of Geology and Geophysics, University of California, Berkeley, California 94720, U.S.A.

ABSTRACT

Perovskites from alkaline intrusions (Africanda, Lovozero, Vuore Yavry, and Sebel Yavry in the Kola peninsula and Karelia and Magnet Cove in Arkansas), carbonatites (Kaiserstuhl, Germany), contact metamorphic and metasomatic rocks (Akhmatov, Urals and San Benito, California) and kimberlites (South Africa) were investigated by electron microprobe and transmission electron microscopy (TEM). Compositions range from almost stoichiometric Ca-Ti oxide (San Benito) to "dysanalite" (= niobian perovskite) with Fe (Magnet Cove and Kaiserstuhl) and loparite with Ce and La (Lovozero). All crystals are orthorhombic and display twinning on {101} and {121}. Rarely APBs with $\mathbf{R} = \frac{1}{2}[010]$ and $\mathbf{R} = \frac{1}{2}[111]$ have been observed, most profusely in "dysanalite" from Magnet Cove and Kaiserstuhl and in loparite from Lovozero. Some perovskites display stacking faults with $\mathbf{R} = \frac{1}{2}[100]$ or $\frac{1}{2}[001]$ and associated partial dislocations of the same Burgers vector. Free dislocations are rare. Most samples show a fine, mottled contrast with directionality. The modulation is more pronounced in samples with deviations from stoichiometry, but we could not document any compositional variations by EDX analyses. We interpret the modulations as inversion boundaries due to slight deviations from centrosymmetry. Defects correspond to those observed in experimentally produced perovskites such as ferroelectrics and high-temperature superconductors, where they were introduced during phase transformations. In the case of the natural perovskites described here, it appears that some defects were introduced by ordering phase transformations (both displacive and chemical) during cooling, and others formed during growth in a nonstoichiometric environment.

INTRODUCTION

The mineral perovskite was originally described by Rose (1839) from metasomatic rocks in the Urals. As early as 1858, Des Cloizeaux observed birefringence that is incompatible with the originally assumed cubic symmetry. Since then, there has been extensive research on perovskite, both natural and synthetic. Of particular importance is the work of Goldschmidt (1926), which discusses the stability range of the perovskite structure as a function of cation radii; of Kay and Bailey (1957), which provides a quantitative refinement of orthorhombic $CaTiO_3$; of Roth (1957) on phase transformations; and of Muller and Roy (1974), with a review of perovskite structures. Perovskite structures have promoted enormous interest because of their applications as ferroelectric materials (e.g., Jaffe et al., 1971) and as high-temperature superconductors (HTS) (e.g., Bednorz and Müller, 1986; Wu et al., 1987). Furthermore, since Liu's (1975, 1976) discovery of high-pressure $MgSiO_3$ perovskite, it has become generally accepted by geophysicists that much of the lower mantle of the Earth is composed of this mineral. Microstructures have been characterized best in ferroelectrics with detailed characterization of planar defects (Randall et al., 1987a, 1987b). There is also an increasing TEM literature on HTS (e.g., Amelinckx et al., 1989) and a very few reports on $MgSiO_3$ (e.g., Guyot et al., 1988; Madon et al., 1980; Wang et al., 1990). Natural perovskites have been largely untouched apart from a study of dislocations (Doukhan and Doukhan, 1986; Poirier and Guyot, 1989). Natural perovskites form under a wide variety of geological conditions and show a wide range of compositions. In this paper, we describe microstructures that are observed in a variety of perovskites.

GEOMETRY OF THE STRUCTURE

The structure of natural perovskites is orthorhombic; the probable space group is *Pnma* with $a = 5.44$ Å, $b = 7.62$ Å, $c = 5.37$ Å. Various settings have been used by different investigators (e.g., *Pcmn* by Kay and Bailey, 1957, and *Pbnm* in most of the materials science literature). We apply here the standard setting to be compatible with computer programs for image simulations and structure reconstruction. It is possible that some natural perovskites are noncentric ($Pna2_1$). Deviations from a cubic structure are small. Figure 1 compares the cubic unit cell ($Pm3m$) with the larger orthorhombic cell (*Pnma*). Transformations of cubic to orthorhombic and ortho-

* On leave from Center for Materials Analysis, Nanjing University, People's Republic of China.

** On leave from Leningrad State University, Leningrad, USSR.

0003–004X/92/0304–0359$02.00

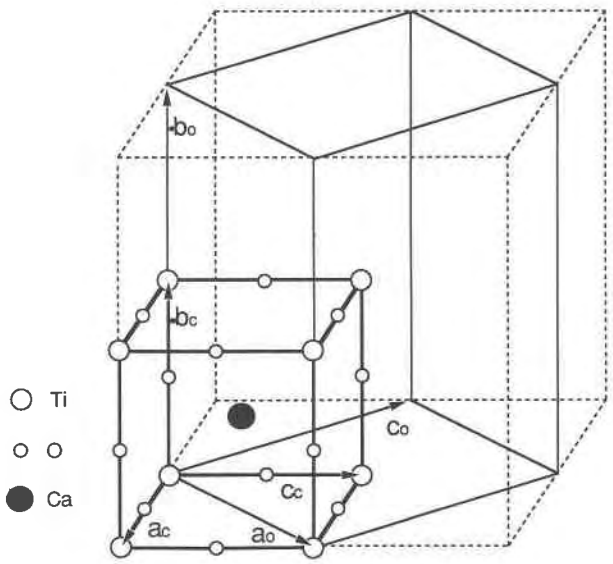

Fig. 1. Schematic sketch of the structure of perovskite comparing the cubic (c) unit cell ($Pm3m$) with the larger orthorhombic (o) unit cell ($Pnma$).

rhombic to cubic Miller indices are

$$\begin{pmatrix} h \\ k \\ l \end{pmatrix}_o = \begin{pmatrix} 1 & 0 & 1 \\ 0 & 2 & 0 \\ -1 & 0 & 1 \end{pmatrix} \begin{pmatrix} h \\ k \\ l \end{pmatrix}_c$$

$$\begin{pmatrix} h \\ k \\ l \end{pmatrix}_c = \begin{pmatrix} 0.5 & 0 & -0.5 \\ 0 & 0.5 & 0 \\ 0.5 & 0 & 0.5 \end{pmatrix} \begin{pmatrix} h \\ k \\ l \end{pmatrix}_o .$$

Corresponding transformations for directions are

$$\begin{pmatrix} u \\ v \\ w \end{pmatrix}_o = \begin{pmatrix} 0.5 & 0 & 0.5 \\ 0 & 0.5 & 0 \\ -0.5 & 0 & 0.5 \end{pmatrix} \begin{pmatrix} u \\ v \\ w \end{pmatrix}_c$$

$$\begin{pmatrix} u \\ v \\ w \end{pmatrix}_c = \begin{pmatrix} 1 & 0 & -1 \\ 0 & 2 & 0 \\ 1 & 0 & 1 \end{pmatrix} \begin{pmatrix} u \\ v \\ w \end{pmatrix}_o .$$

Mainly because of small displacements of Ca and O atoms from cubic positions, b is doubled and a and c are no longer equivalent; this is apparent in projections of the crystal structure (Fig. 2). There is no information about the detailed cation distribution in nonstoichiometric natural perovskites, in part because it is difficult to determine such distributions with X-ray techniques because of submicroscopic twinning. Figure 3 shows a stereographic projection of symmetry elements in cubic and orthorhombic perovskite. We see that cubic (110), ($\bar{1}$10), (011), (0$\bar{1}$1), (100), and (001) mirror planes are not present in the orthorhombic structure and are therefore obvious twin planes in orthorhombic perovskite as two nonequivalent systems {121} and {101}. Since $a_o \approx c_o \approx \sqrt{2}/2b$, several different lattice planes hkl have almost identical d values, and indexing of selected area diffraction patterns (SAD) is often ambiguous. The most reliable identification is in $hk0$, $h0l$, and $0kl$ SADs, which are unique because of systematic absences. But even in those, there is often ambiguity because of double diffraction (which can be reduced by analyzing thinner parts of the foil), contributions from microtwins (which can be ascertained by dark-field imaging), and the cubic pseudosymmetry. For example, a [100] zone axis diffraction pattern is almost identical to one with a [$\bar{1}$1$\bar{1}$] zone axis. Figure 4 illustrates diffraction patterns in the three main orthorhombic directions (Figs. 4a–4c) and the pseudocubic directions (Figs. 4d–4f). Unless indicated, all indices (hkl)[**uvw**] refer to the orthorhombic unit cell for $Pnma$. Some important correspondences between cubic and orthorhombic indices are

cubic ($Pm3m$)	orthorhombic ($Pnma$)
{100}	{101}, (020)
{110}	(200), (002), {121}
{111}	{022}, {220}
⟨100⟩	[010], ½⟨101⟩
⟨101⟩	[100], [001], ⟨111⟩
⟨111⟩	⟨210⟩, ⟨012⟩.

Sample descriptions and analytical techniques

In choosing samples for this study, we tried to cover the different petrologic associations in which perovskite occurs. The following paragraphs describe the geological setting. Corresponding electron microprobe analyses are listed in Tables 1 and 2. In addition to the elements shown in these tables, we analyzed for K and U but found no significant amounts. The low totals in some of the samples indicate that some additional elements, particularly other rare earths, may be present.

Alkaline magmatism. The Kola-Karelian area in the eastern part of the Baltic shield is a classical province of ultrabasic-alkaline magmatism, active in Caledonian and Hercynian time. The Caledonian massifs consist of complicated multiphase intrusions with a combination of conical bodies. The parental magma is undersaturated in Si and Al and rich in Mg, Ca, and Na. The evolution of the magma is uniform from ultramafic through alkaline to carbonatite. Titano-magnetite and perovskite mineralization is associated with the early ultramafic stage; aegirine, forsterite, melilite, wollastonite, and sodalite with the alkaline series; and rare baddeleyite and pyrochlore (koppite) with carbonatites. We investigated samples from Africanda where perovskite occurs as large twinned crystals in coarse pyroxenite. It is rich in Ce and other rare earths (knopite), and some Nb substitutes for Ti (Table 1). Perovskites from Vuore Yavry occur in two generations in diopside-pyroxenite with titano-magnetite. The first generation is coarser with a lower Ce and rare earth content; the second generation is smaller and distinctly zoned, the edge enriched in rare earths and Nb as is illustrated with a microprobe scan for Nb over a zoned

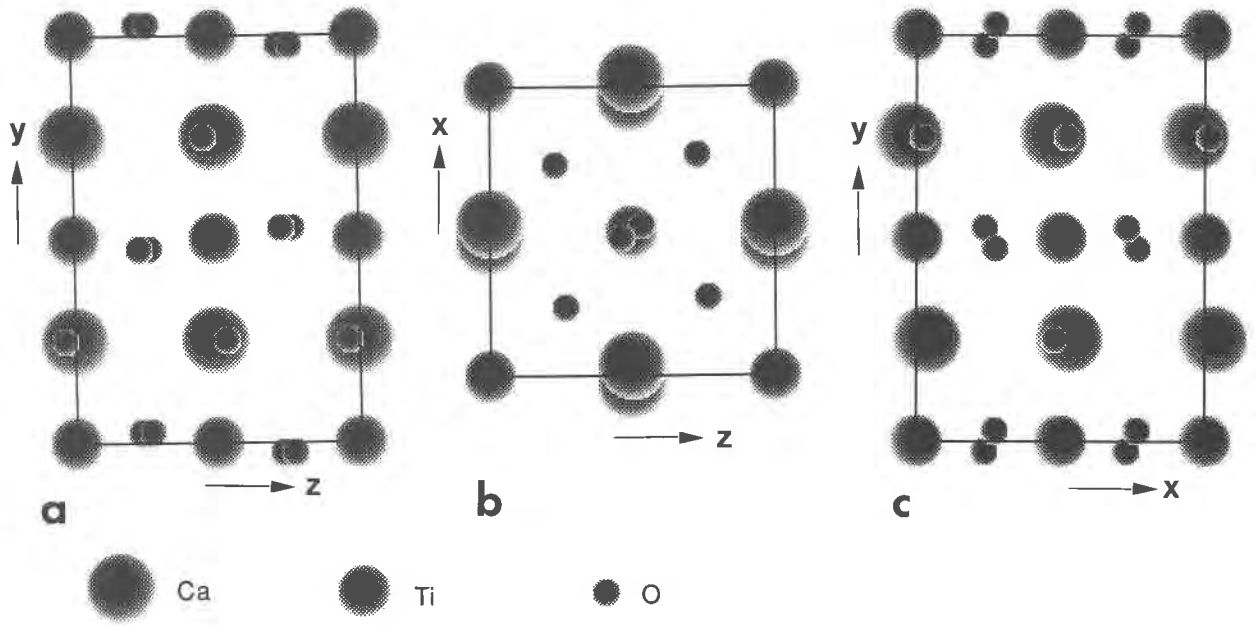

Fig. 2. Projections of the structure of orthorhombic perovskite, illustrating atomic displacements, particularly of O atoms (atomic parameters from Kay and Bailey, 1957). The size of atoms is roughly proportional to their scattering power; (**a**) [100] projection, (**b**) [010] projection, (**c**) [001] projection.

grain (Fig. 5a). Whereas Ce is the most abundant rare earth element, it was possible to document minor amounts of Nd, Pr, and La (Fig. 5b). Perovskites from Sebel Yavry are fine grained and again associated with titanomagnetite. The crystals chosen for our analysis are from a phlogopite layer, and compositionally they are close to stoichiometric perovskite (Bulakh and Abakumova, 1960).

Hercynian peralkaline nepheline-syenite plutons located in the central Kola peninsula display rhythmic subhorizontal layering (Sörensen, 1969). Rocks are rich in Na, Al, Ca, F, Cl, Nb, Ti, and rare earths (Nefedov, 1938). A perovskite sample from the Lovozero massif is exceptionally rich in Ce (loparite) and Nb (Bykova, 1941).

Perovskites from alkaline intrusions in the Kola peninsula were compared with "dysanalite" from the central part of the Mesozoic Magnet Cove massif in Arkansas (Washington, 1900). Large octahedral crystals are profusely twinned and display sector zoning.

We also examined "dysanalite" in Tertiary carbonatites from Badloch associated with the alkaline Kaiserstuhl intrusion (southern Germany, e.g., Knop, 1877; Hauser, 1908; Meigen and Hügel, 1913; Wimmenauer, 1963). In these carbonatites Nb occurs in perovskites and koppite ($Ca_2Nb_2O_7$).

Contact metamorphism and metasomatism. In the Nazamsky Mountains of the Urals, contact metamorphism in talc-chlorite schists and limestones around dioritic intrusions produced rich mineralogical assemblages. A sample from mines in Akhmatov (the locality at which Rose, 1839, discovered the mineral) is in marble, associated with garnet, apatite, and chlorite (Bonstedt, 1935). Compared with compositions of perovskites from alkaline intrusions, those from Nazamsky are relatively stoichiometric.

Along the southern contact of the San Benito serpentinite massif, California, are strongly metasomatized

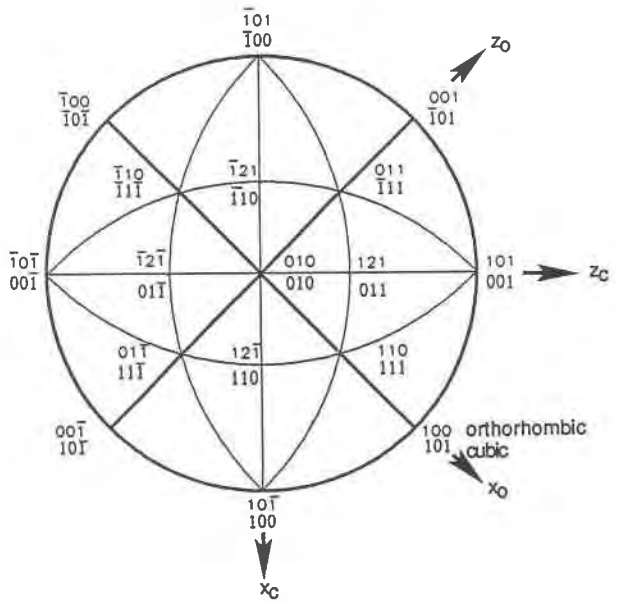

Fig. 3. Lower hemisphere stereographic projection of important planes in cubic and orthorhombic perovskite. Heavy lines indicate mirror planes in orthorhombic perovskite. Thin lines are mirror planes in cubic perovskite but not in orthorhombic perovskite and are potential twin planes. Indices are on top for the orthorhombic and below for the cubic setting.

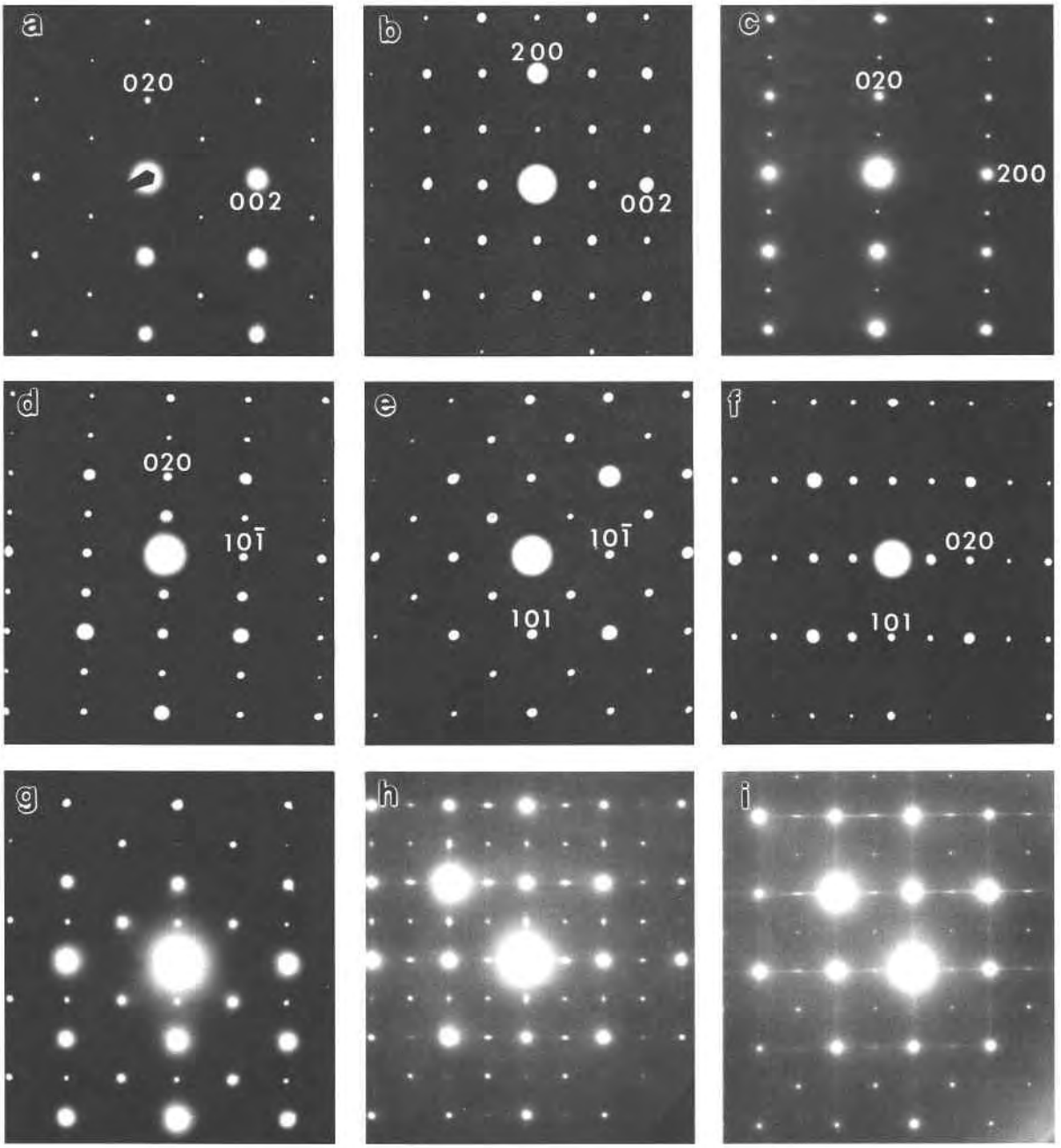

Fig. 4. Electron diffraction patterns of perovskite. Top: diffraction patterns along the three main orthorhombic axes (**a**) 0*kl*, (**b**) *h*0*l*, (**c**) *hk*0. Center: diffraction patterns along the three pseudocubic axes. Bottom: diffraction patterns of twins, (**g**) (101) twin, two variants (a combination of **a** and **c**); (**h**), (**i**) (121) twins in "dysanalite" from Lovozero with three variants [a combination of (**d**), (**e**), and (**f**)]. In **i** a high density of APBs gives rise to diffuse streaking along **b***. All indices shown refer to the orthorhombic unit cell (*Pnma*).

chlorite schists with development of such Ti minerals as titanium melanite, benitoite, neptunite, and almost stoichiometric perovskite (e.g., Murdoch, 1951; Pabst, 1951).

Kimberlites. Finally, perovskites occur in kimberlites. We surveyed with the TEM perovskite occurring as fine (0.1–0.5 mm) crystals in the groundmass of olivine magnetite melilites from Namaqualand, South Africa (Moore, 1981; Haggerty et al., 1985). EDX analysis in the TEM indicated only a minor rare earth content.

After initial characterization of the samples by optical microscopy and chemical analysis of major components by electron microprobe, we prepared foils for TEM analysis by ion beam thinning. This was straightforward for large crystals but difficult for fine-grained aggregates, such

TABLE 1. Electron microprobe analyses of perovskites

Locality	CaO	Na_2O	Ce_2O_3	La_2O_3	TiO_2	Nb_2O_5	FeO	Al_2O_3	Total
Africanda	35.86	0.91	2.73	1.32	54.78	1.56	1.37	0.16	98.77
Vuore Yavry									
1. Generation core	38.56	0.36	1.25	0.49	57.00	0.44	0.76	0.12	98.99
rim	38.15	0.43	1.41	0.80	56.51	0.58	0.89	0.12	98.88
2. Generation	37.78	0.47	1.64	0.82	55.65	0.60	0.99	0.12	98.21
Sebel Yavry	39.14	0.23	0.99	0.42	57.58	0.40	0.86	0.11	99.78
Lovozero	5.02	8.80	19.78	11.59	42.65	6.44	0.50	0	94.80
Magnet Cove	36.03	0.37	1.72	1.29	40.11	10.32	5.54	0.61	96.09
Kaiserstuhl	30.07	2.60	1.57	0.82	37.58	19.08	4.07	0.16	96.06
Akhmatov	39.59	0.02	1.01	0.59	57.12	0.21	1.12	0.04	99.79
San Benito	40.30	0.11	0.36	0.17	58.48	0.24	0.24	0	99.97

Note: Weight percent oxides. Analyses performed on polished grain mounts with an automated ARL-SEMQ microprobe operated at 30 nA and 15 kV, eight single-channel spectrometers, using eight oxide standards and correcting with a modified ϕ-ρ-z Armstrong method.

as those from kimberlites, because perovskite proved to be much more resistant to thinning than other components, prohibiting development of thin edges of the TEM foil.

Most of the TEM work was done with a JEOL 100C in the Department of Geology and Geophysics, UC–Berkeley, making extensive use of dark-field imaging. We performed more detailed analyses on selected samples at the National Center for Electron Microscopy of Lawrence Berkeley Laboratory; in particular, we investigated local compositional variations with a JEOL 200CX STEM and structural heterogeneities with the atomic resolution JEOL ARM 1000, and we performed in situ heating experiments in the Kratos 1.5 MeV HVEM.

Identification of defects

The samples of perovskite that we investigated display a surprisingly wide variety of planar defects, which are summarized in Table 3 and described in more detail below. For each sample we investigated several foils and different areas. In Table 3 we indicated those microstructures that we have identified, which does not exclude that others may be present.

Twinning. Whenever a structure of higher symmetry degenerates into one of lower symmetry by loss of rotational symmetry elements, twinning can result. In perovskite, two twin systems are likely. The system {121} with three orientation variants is due to the doubling of the *b* axis, e.g., as a result of the transformation of cubic to tetragonal perovskite; any of the three cubic axes can assume the long *b* dimension. The twin system {101} with two variants is due to loss of equivalence between cubic *a* and cubic *c*, i.e., it occurs during the transformation from tetragonal to orthorhombic symmetry (Fig. 3 of Bowman, 1908). When viewed with a petrographic microscope, all perovskites examined in this study do show twinning. However, there is a considerable variation in twin density. Least twinning is observed in the almost stoichiometric San Benito and Namaqualand specimens, and profuse twinning occurs in large Ce-rich crystals from Vuore Yavry and Africanda. A correlation of twin densities with deviations from stoichiometry was previously noted by Holmquist (1897).

With the TEM we mainly observed fairly large twins (>5 μm), widely spaced, corresponding to those observed with the optical microscope. Isolated microtwins, less than 1 μm in width, are also not uncommon. Figure 6 shows inclined (101) microtwins in perovskite from Africanda. The twin plane is (101), and the normal to (101) is the twin axis. Such twins can also be viewed as originating through a 90° rotation around **b**. The composite diffraction pattern of host (H) and twin (T) (bottom right in Fig. 6) appears like a single reciprocal lattice with superstructure reflections. Because of the cubic pseudosymmetry and similarity in lattice parameters, many reflections coincide, and splitting is only observed at high diffraction

TABLE 2. Electron microprobe analyses of perovskites

Locality	Ca	Na	Ce	La	Ti	Nb	Fe	Al
Africanda	0.905	0.042	0.024	0.011	0.972	0.017	0.028	0.004
Vuore Yavry								
1. Generation core	0.956	0.016	0.011	0.004	0.991	0.005	0.015	0.003
rim	0.950	0.019	0.012	0.007	0.987	0.006	0.017	0.003
2. Generation	0.950	0.022	0.014	0.007	0.983	0.006	0.019	0.003
Sebel Yavry	0.961	0.010	0.008	0.004	0.992	0.004	0.016	0.003
Lovozero	0.157	0.497	0.211	0.124	0.934	0.084	0.012	0
Magnet Cove	0.978	0.018	0.016	0.012	0.764	0.118	0.117	0.018
Kaiserstuhl	0.820	0.128	0.015	0.008	0.719	0.220	0.087	0.005
Akhmatov	0.975	0.001	0.008	0.005	0.987	0.002	0.022	0
San Benito	0.981	0.005	0.003	0.001	0.999	0.002	0.005	0

Note: Formulas normalized to three O atoms (compare Table 1).

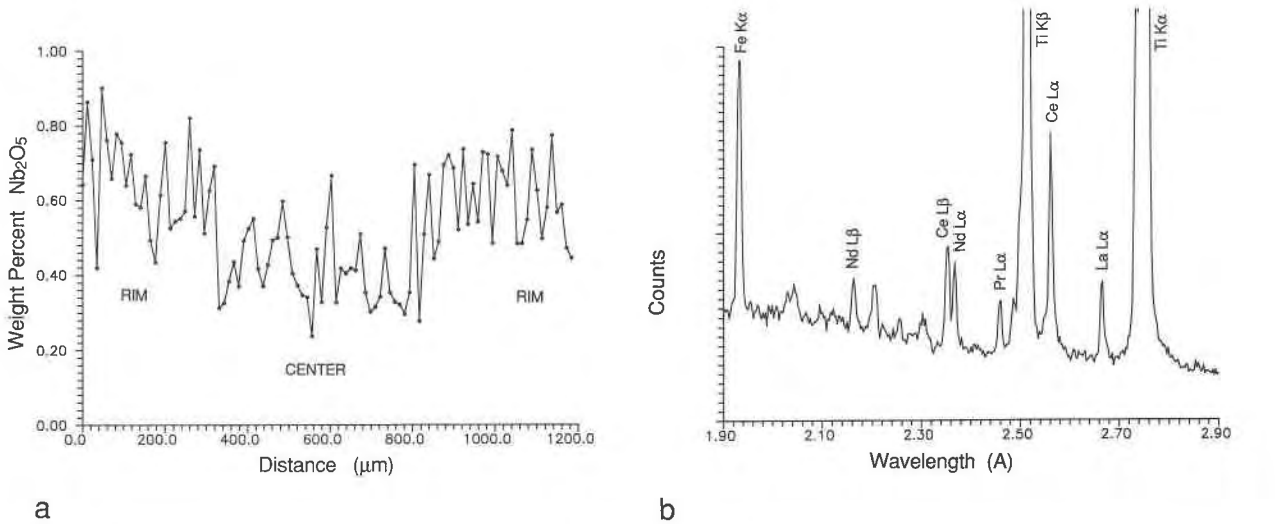

Fig. 5. Electron microprobe analyses of perovskite from Vuore Yavry. (**a**) Traverse over a zoned grain with enrichment of Nb_2O_5 near the rim. (**b**) Wavelength scan illustrating presence of Ce, Nd, Pr, and La.

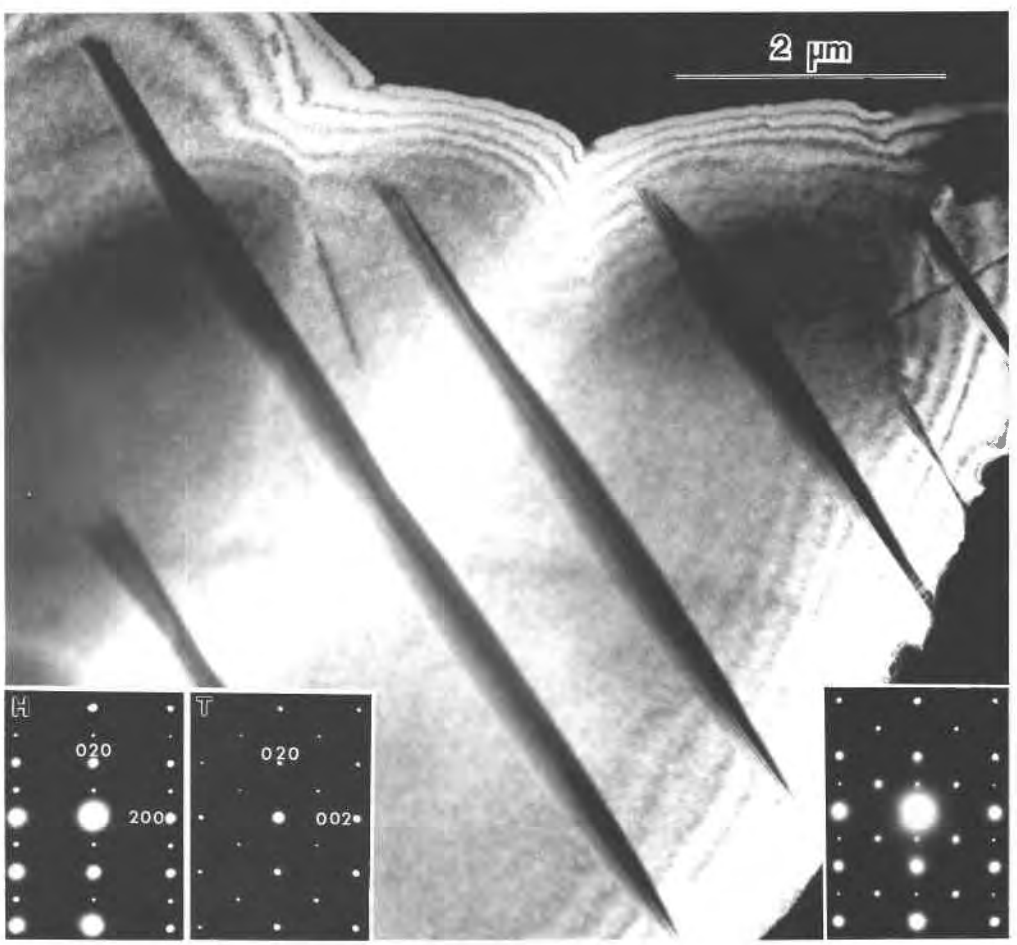

Fig. 6. Some (101) microtwins in perovskite from Africanda. Inserted diffraction patterns in a different orientation illustrate orientation of host, which constitutes the main volume (H), and thin twins with fringes (T) (lower left) and a composite pattern (lower right).

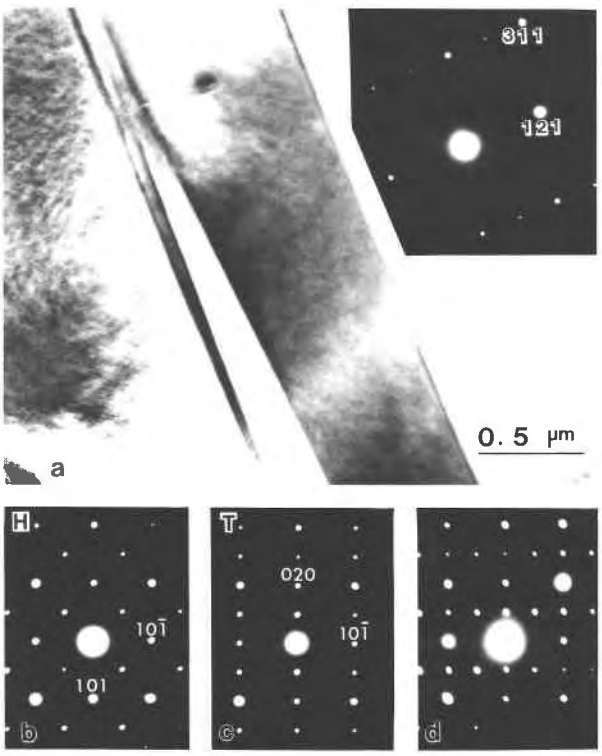

Fig. 7. A (121) twin in perovskite from Magnet Cove viewed edge-on. Diffraction patterns at the bottom are in a different orientation than the image on top (**a**), illustrating (**b**) host (H), (**c**) twin (T), and composite of both (**d**).

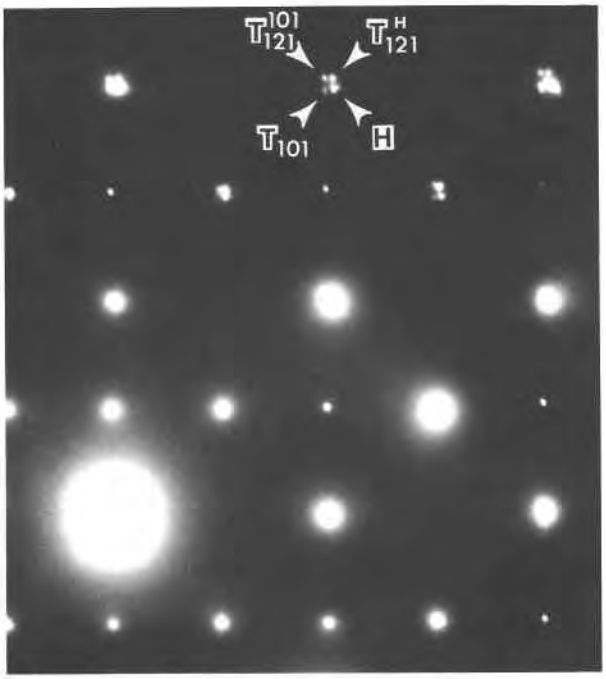

Fig. 8. Magnet Cove sample: selected area diffraction pattern of (101) and (121) twins in the same grain with splitting of reflections at higher order. Four variants result: host H, 110 twin T_{110}, and both host and 110 twin twinned on 121 T_{121}.

angles. Figure 7 illustrates a (121) twin in "dysanalite" from Magnet Cove viewed edge-on. The diffraction patterns at the bottom are not in the same orientation as the image above, but they illustrate again the near coincidence of the two reciprocal lattices. Figure 7b is the diffraction pattern of the host (H), Figure 7c is that of the twin (T), and Figure 7d is the composite diffraction pattern; (121) twins have (121) as the twin plane and the normal to (121) as the twin axis. They can be viewed as a 90° rotation around [101]. Figures 4g–4i illustrate some twinned diffraction patterns, Figure 4g is a (101) twin (a combination of Figs. 4a and 4c), and Figures 4h and 4i are (121) twins with three variants (a combination of Figs. 4d, 4e, and 4f), again giving the impression of a single superlattice. Sometimes splitting of high-order reflections is observed. Figure 8 shows an interesting diffraction pattern with contributions from four twin domains, both (101) and (121). In none of the many samples that we analyzed could we find any parallel (101) twins with the twin axis parallel, rather than normal, to the twin plane. Those have been classified as 90° twins by Bowman (1908) and are apparently rare in the samples investigated here. Composition planes are nearly parallel to twin planes, but frequently they are slightly curved. The {121} twins are more common than {101} twins, which may be due to the higher multiplicity of {121} or to the lower strain energy (Randall et al., 1987b). Microtwins less than 0.1

Table 3. Summary of microstructural observations in natural perovskites

	Twins		APBs		Stacking faults	Dislocations	Mottled contrast	Short range order
	121	101	½[010]	½[111]				
Africanda	X	X		X			X	
Vuore Yavry	X	X		X		(X)	X	
Sebel Yavry	X	X					X	
Lovozero	X	X		X			(X)	X
Magnet Cove	X	X	X	X		(X)	X	
Kaiserstuhl	X	X	(X)	X			(X)	
Akhmatov	X	X	(X)		X	(X)	X	
San Benito	(X)	(X)						
Namaqualand	(X)	(X)						

Note: (X) indicates that structure is poorly developed or rare.

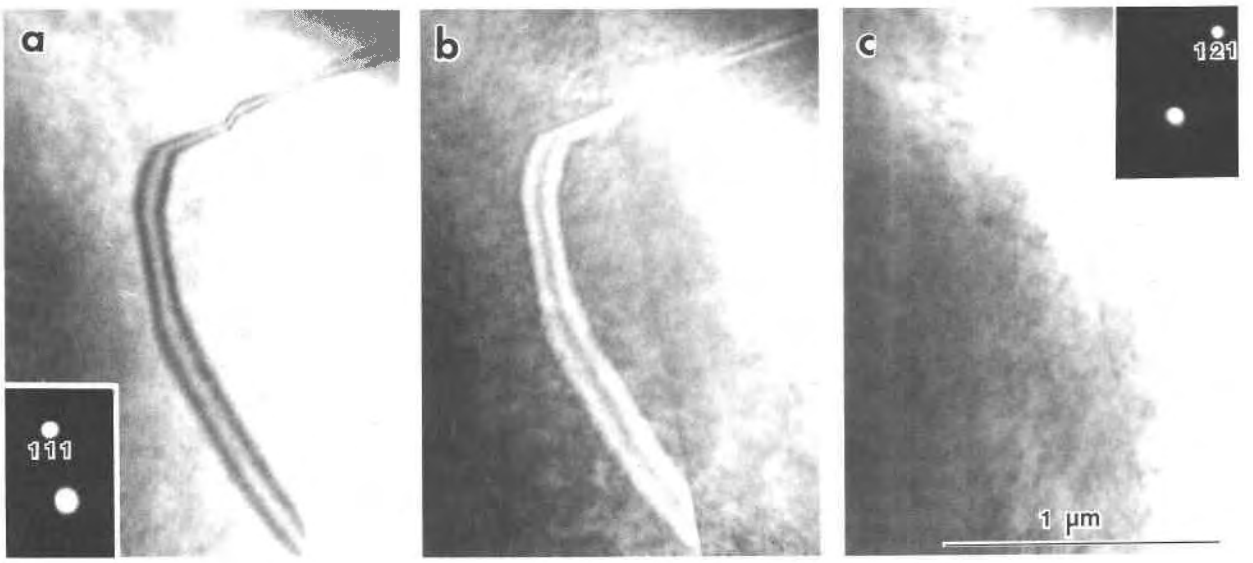

Fig. 9. Antiphase boundary with symmetrical fringes in perovskite from Akhmatov (Urals). Contrast analysis with two-beam condition, the operating **g** vector is indicated; (**a**, **b**) in contrast for 111, (**c**) out of contrast for 121 (**a**, **c** are bright-field images, **b** is a dark-field image).

μm in width are relatively rare and their spacing is irregular with the host orientation always dominating (Fig. 6), which we interpret as evidence that many twins form during growth rather than during a phase transformation from a cubic parent. Never did we observe polysynthetic microtwins such as occur in microcline.

Antiphase boundaries. Whereas loss of rotational symmetry elements from the cubic parent structure gives rise to twinning, loss of translational symmetries may introduce antiphase boundaries (APBs). Doubling of b is a likely source of APBs in orthorhombic and tetragonal perovskites. We have found some widely spaced, curved APBs in perovskite from Akhmatov, but they are rare. Contrast analysis (Fig. 9 and Table 4) shows that APBs are in contrast for reflections (hkl), k = odd such as 111 (Figs. 9a, 9b), and out of contrast for reflections k = even such as 121 (Fig. 9c), consistent with a displacement vector $\mathbf{R} = \frac{1}{2}[010]$. Notice the symmetrical fringes both in bright field (Fig. 9a) and in dark field (Fig. 9b) with a bright center fringe in bright field. Associated partial dislocations have a Burgers vector $\mathbf{b} = \frac{1}{2}[010]$.

Table 4. Visibility of antiphase boundary (APB) and dislocation in perovskite from Akhmatov as a function of the reflection used for imaging in the two-beam condition

Reflection **g** (*hkl*)	APB **R** = ½[010]	Dislocation **b** = ½[010]
(111)	in	in
(121)	out	in
(042)	out	in
(222)	out	in
(101)	out	out
(202)	out	out
(012)	in	in

Note: in = in contrast, out = out of contrast.

Very complicated defects were observed in "dysanalite" from Magnet Cove. Figure 10 shows in dark field a microstructure with a (101) twin. Contrast analysis documents two types of APBs (Table 5). One set of APBs has a displacement vector $\mathbf{R} = \frac{1}{2}[010]$, the same as those described above. However in the Magnet Cove "dysanalite," they are not irregularly curved as in perovskite from Akhmatov but instead are aligned parallel to (101) and are therefore conservative. A second set of APBs has a displacement vector $\mathbf{R} = \frac{1}{2}[111]$. These boundaries have two morphologies, one is along $(1\bar{1}0)$, again conservative, and the second along (100), which is nonconservative. Both displacement vectors, $\frac{1}{2}[010]$ and $\frac{1}{2}[111]$, are lattice vectors in the cubic cell (Fig. 1). At the intersection of two APBs we observe a partial dislocation with a Burgers vector $\mathbf{b} = \frac{1}{2}[101]$, which we interpret as a stair-rod dislocation resulting from the reaction $\frac{1}{2}[010] + \frac{1}{2}[1\bar{1}1] =$

Table 5. Visibility of antiphase boundaries (APB), dislocations, and modulated structure in perovskite from Magnet Cove as a function of the reflection used for imaging in a two-beam condition

Reflection **g** (*hkl*)	APB **R** = ½[111]	APB **R** = ½[010]	Dislocation **b** = ½[101]	Modulated structure
(111)	in	in	in	in
(121)	out	out	out	in
(101)	out	out	out	in
(114)	out	in	in	in
(002)	out	out	in	out
(201)	in	out	in	in
(112)	out	in	in	in
(122)	in	out	in	out
(220)	out	out	in	out
(012)	in	in	in	out
(131)	in	in	out	in

Note: in = in contrast, out = out of contrast.

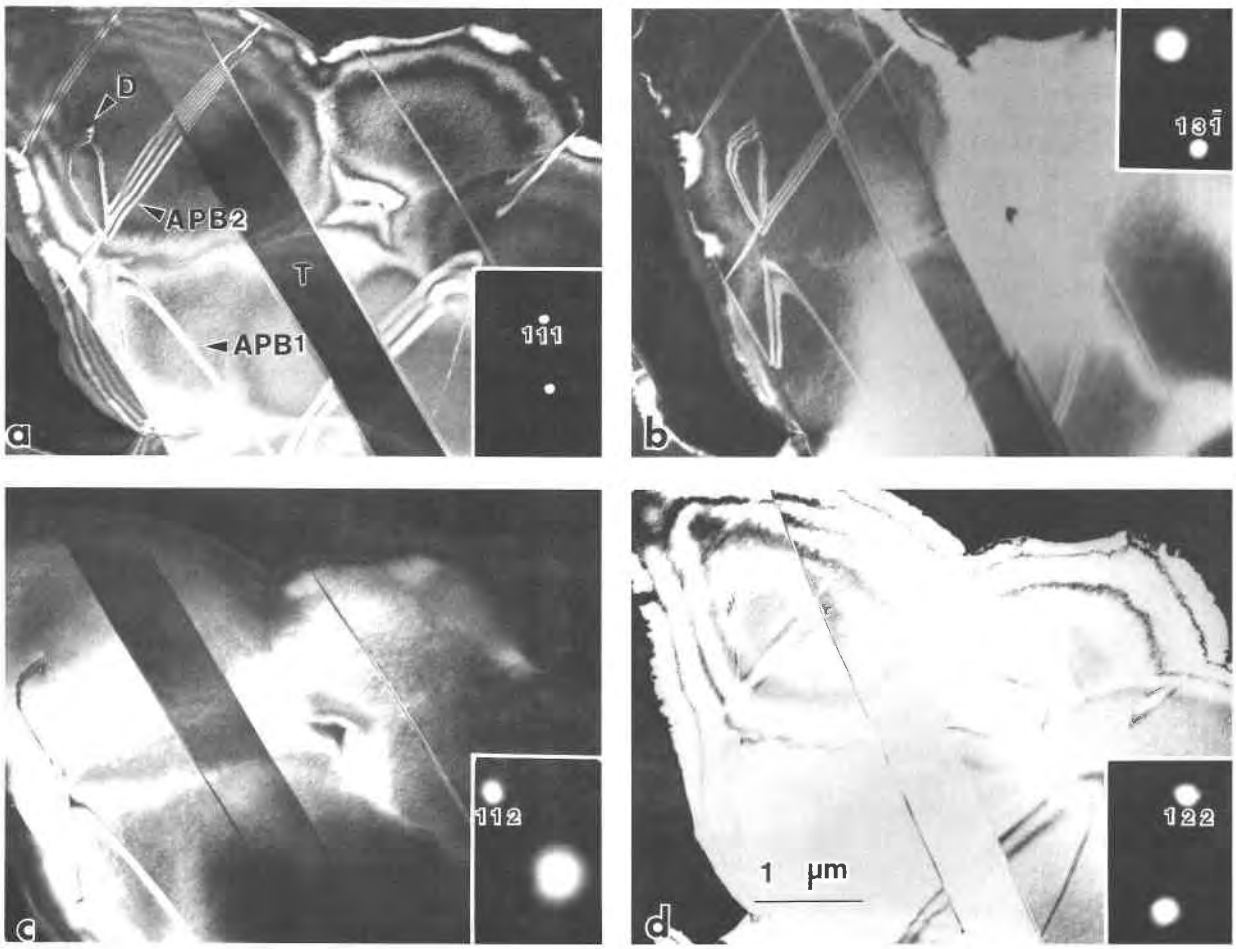

Fig. 10. Defects in "dysanalite" from Magnet Cove. (**a–d**) Same area in different contrast conditions in dark field. Operating **g** vectors are indicated in the inserted diffraction patterns. Diagonal (101) twin (T), **R** = ½[010] APB (APB1) and **R** = ½[111] APB (APB2). At the intersection of the two APBs is a partial dislocation with **b** = ½[101] (D).

½[101]. The Burgers vector $[110]_c$ = ½[111] has also been observed by Prisedsky et al. (1985) in lead titanate (PZT).

The most profuse domain structure is present in loparite from Lovozero. In some areas APBs are irregularly curved (Fig. 11), but generally they are elongated in the (010) plane and produce diffuse streaking along **b*** in the diffraction pattern. The curved APBs of Figure 11 resemble closely those observed in synthetic lead perovskites introduced during a phase transformation (Randall et al., 1986; Baba-Kishi and Barber, 1990). Figure 12 displays two sets of {121} twins with fairly irregular twin boundaries and three orientation variants. The composite diffraction pattern is shown in Figure 4i with two sets of diffuse streaks. Reflections that are streaked are of the type h and k even, l = odd. With dark-field analysis we could image APBs in domains A and C. Contrast analysis confirms again a displacement vector **R** = ½[111] and not ½[010] as one might expect based on the morphology. Notice the change in morphology across the twin plane, which is evidence that APBs formed after or simulta-

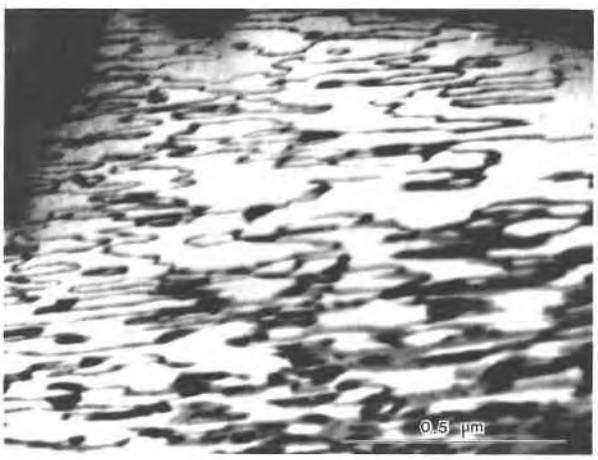

Fig. 11. Curved ½[111] APBs in loparite from Lovozero, dark-field image with 121 operating.

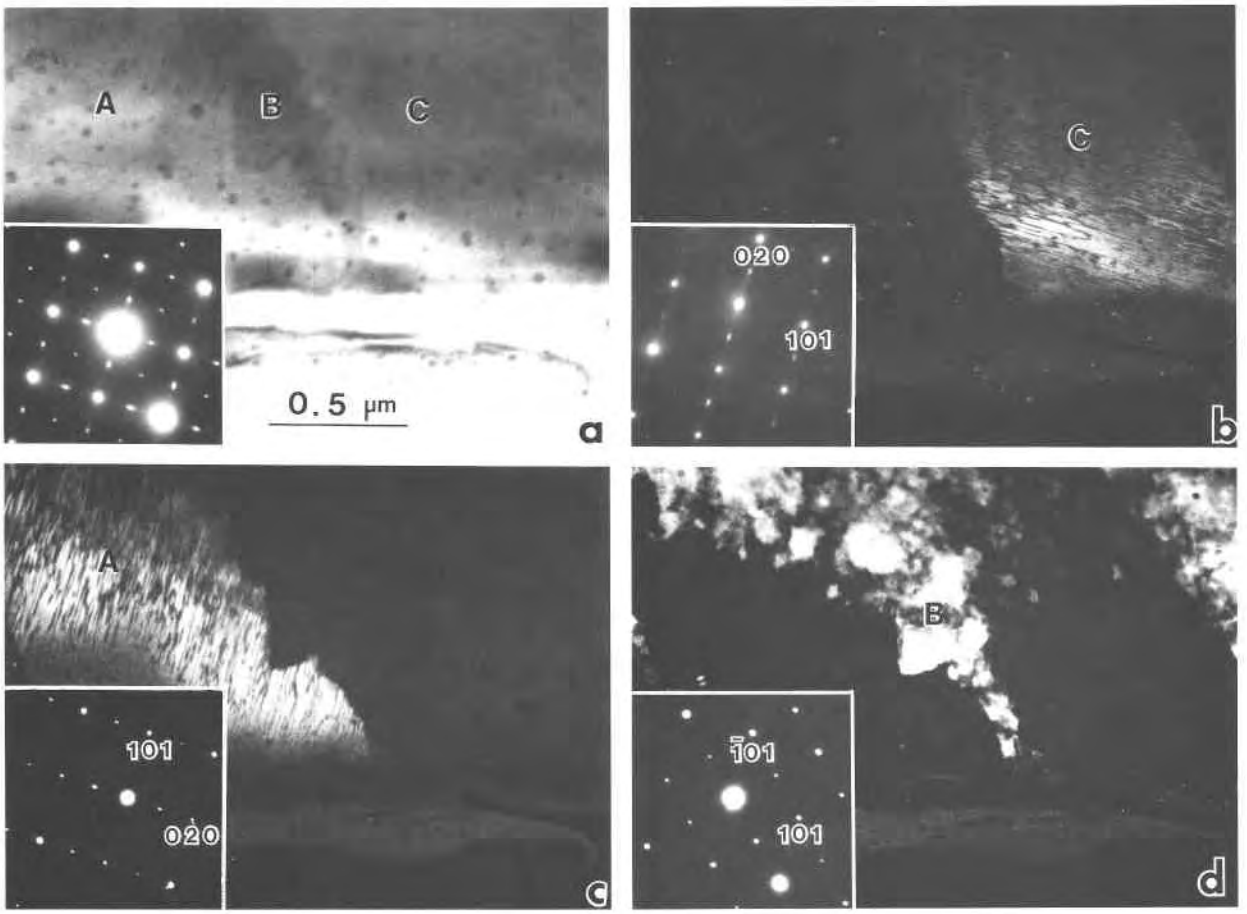

Fig. 12. Loparite from Lovozero with three (121) twin orientation variants A, B, and C. The diffraction pattern inserted in the bright-field image (**a**) is a superposition over all three regions. Diffraction patterns inserted in the dark-field images (**b**), (**c**), and (**d**) with **g** vectors indicated are from the individual areas. Aligned $\mathbf{R} = \frac{1}{2}[111]$ APBs are in contrast in areas A and C. Compare with this figure also the diffraction pattern in Figure 4i.

neously with the twins. These APBs are partially nonconservative, and since they occur in high numbers they are capable of accommodating nonstoichiometry in this Nb-Ce-rich sample.

Figure 13 shows a (121) twin in the same sample but with a different orientation. Again we observe $\frac{1}{2}[111]$ APBs elongated in the (010) plane. In this case a fine modulated structure is in strong contrast. Also in the diffraction pattern there is a conspicuous diffuseness. We have done a preliminary survey of Lovozero loparite with the atomic resolution TEM and observed clustering in thin areas in [010] images (Fig. 14), which we think is due to short-range order in the cation distribution. Since the contrast increases in very thin areas of the foil, it is due to atomic occupancies rather than unit-cell distortions. Similar short-range order was observed by Krause et al. (1979) in lead magnesium niobates. The diffuseness in Figure 13 may be related to such short-range order.

"Dysanalite" from Kaiserstuhl is comparable to that from Magnet Cove, again with APBs that show rather strong crystallographic alignment, particularly parallel to (101), e.g., along twins (Fig. 15a). In atomic resolution micrographs we documented conservative (Fig. 15b) and nonconservative APBs (Fig. 15c).

Stacking faults. Stacking faults with asymmetric fringes have been observed in perovskite from Akhmatov (Fig. 16). The displacement vector is $\mathbf{R} = \frac{1}{2}[001]$ or $\frac{1}{2}[100]$, which is the same as the Burgers vector of the partial dislocations. Such a displacement brings O atoms to coincidence but displaces cations. Stacking faults are in the (010) plane and therefore conservative. The Burgers vector of the dislocations corresponds to $\frac{1}{2}[101]_c$, which Doukhan and Doukhan (1986) described in $BaTiO_3$. It was proposed by Poirier and Guyot (1989) that such displacements prevent cations from coming in close contact during movements of dislocations. Prisedsky et al. (1985) interpret planar defects with $\mathbf{R} = \frac{1}{2}[110]_c$ in $Pb(Ti,Zr)O_3$ (PZT) as crystallographic shear planes associated with nonstoichiometry.

Mottled contrast. In all samples we observed a mottled contrast. This contrast is sometimes fine with a wavelength of 200 Å (Figs. 17a, 17c), sometimes coarser

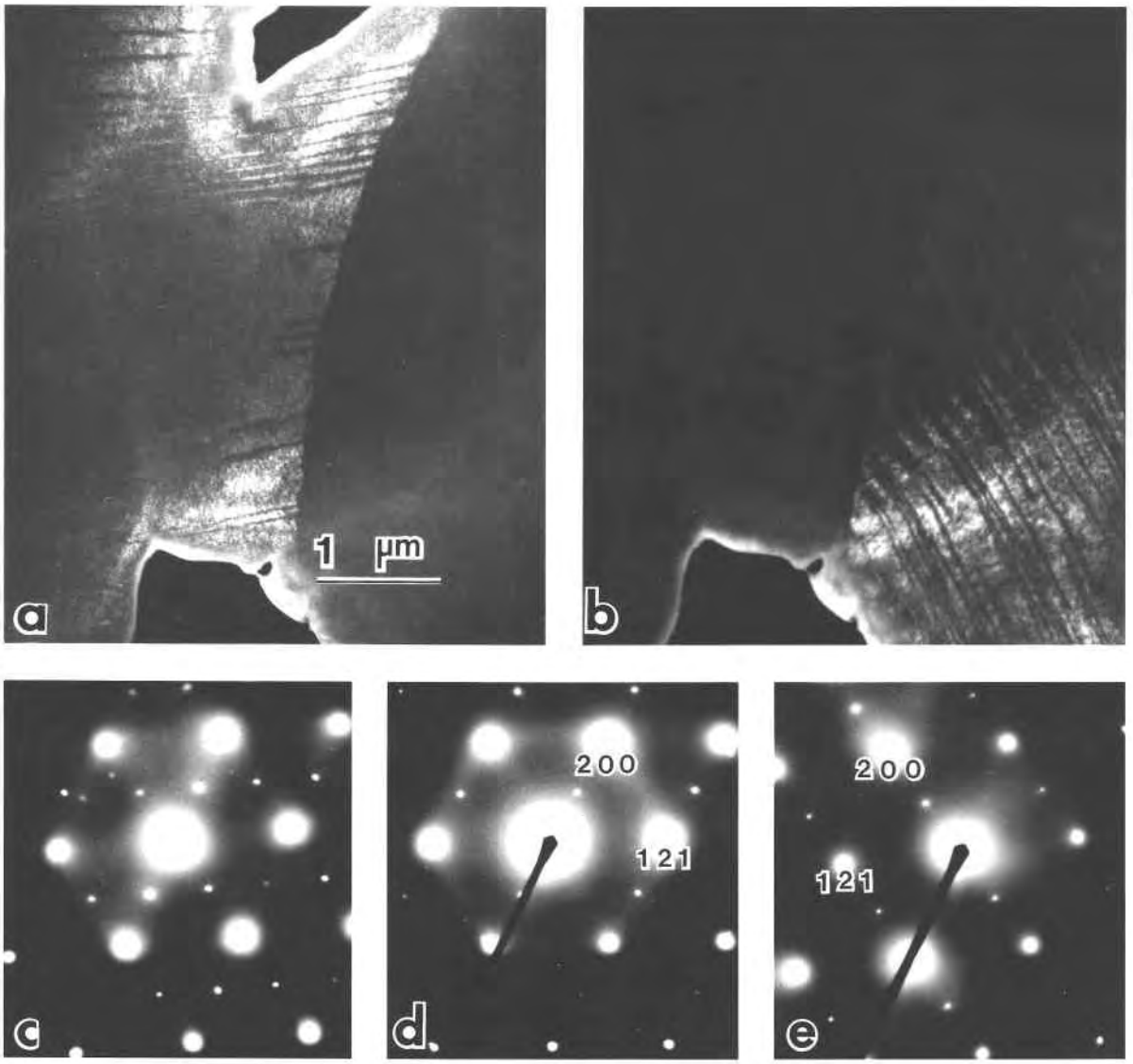

Fig. 13. Loparite from Lovozero with (121) twin. Dark-field images show APBs and a fine modulated structure in contrast in different regions, (**a**) and (**b**). (**c**) Composite diffraction pattern including region **a** and **b**, (**d**) corresponds to **a**, and (**e**) corresponds to **b**. Notice the diffuse intensity, particularly visible in **d**.

up to 2000 Å (Fig. 17b). It is often irregular (Fig. 17b) and occasionally shows directionality (Fig. 17c), most often elongated close to [010]. The modulation shows strong contrast with basic reflections of the cubic perovskite structure, but there are reflections with which contrast is weak (Table 5). We have been unable so far to associate the structure in the image with diffraction evidence such as diffuseness or streaking shown in Figure 13, which occurs in areas with strong modulations. We ascertained that the contrast is not an artifact introduced during ion beam thinning or electron beam damage. We note that a similar contrast was observed in PIN ferroelectrics at low temperature (Randall et al., 1987a, 1987b). Even though evidence is inconclusive, we suggest that this black-white mottled contrast is due to inversion boundaries that are an expression of slight deviations from centrosymmetry (Hu et al., 1982; Hu and Fong, 1982). As an electron beam travels through an oblique inversion boundary, it passes from a positive domain (with a $+\mathbf{g}$ deviation) into a negative domain (with a $-\mathbf{g}$ deviation) or vice versa. Depending on whether the beam enters first the positive or negative domain, the superposed contrast is either bright or dark, similar to that in Figure 17b.

Conclusions

All defects that have been observed in natural perovskites are readily understood in terms of the pseudocubic crystal structure. Twins, APBs, stacking faults, inversion

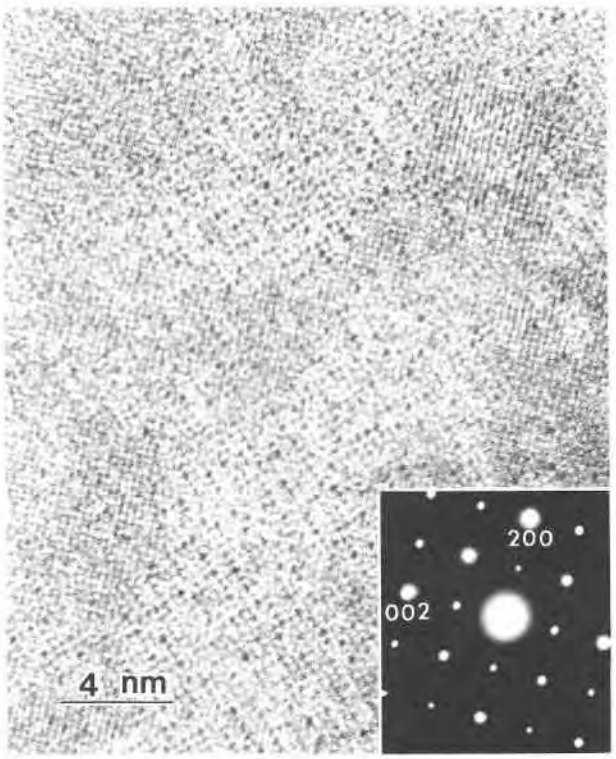

Fig. 14. Loparite from Lovozero. Multibeam phase contrast atomic resolution image along [010] illustrating a highly irregular cation distribution in clusters indicative of short-range order.

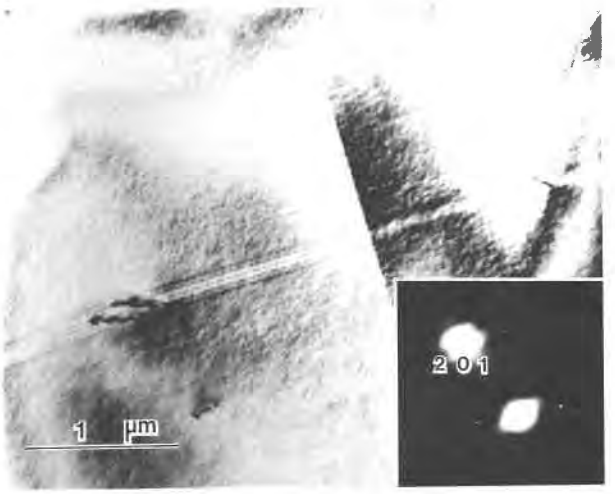

Fig. 16. Dark-field image of a ½[100] stacking fault with symmetrical fringes and dislocations in perovskite from Akhmatov. Two-beam condition with 201 operating.

boundaries, and dislocations could form during phase transformations from a more highly symmetrical to a lower symmetry structure. Phase transitions have been well studied in $BaTiO_3$ (e.g., Kay and Vousden, 1949), which transforms at 110 °C from cubic to tetragonal, doubling the *b* lattice parameter as a result of slight atomic displacements. Such a transition could give rise to ½[010] APBs and to {121} twins because of the translational and rotational symmetry elements lost during the transition. On further cooling, below 0 °C, the tetragonal structure becomes orthorhombic. Here the $\frac{1}{2}[101]_o = [100]_t$ translation is lost as is the $\{101\}_o = \{100\}_t$ mirror planes, giving rise to corresponding APBs (or stacking faults) and twins. Also during that transformation, ½[010] APBs may decompose into nonequivalent $\frac{1}{2}[001]_o$ and $\frac{1}{2}[111]_o$ APBs, both of which were observed in the investigated natural perovskites. Finally, below −100 °C, orthorhombic bar-

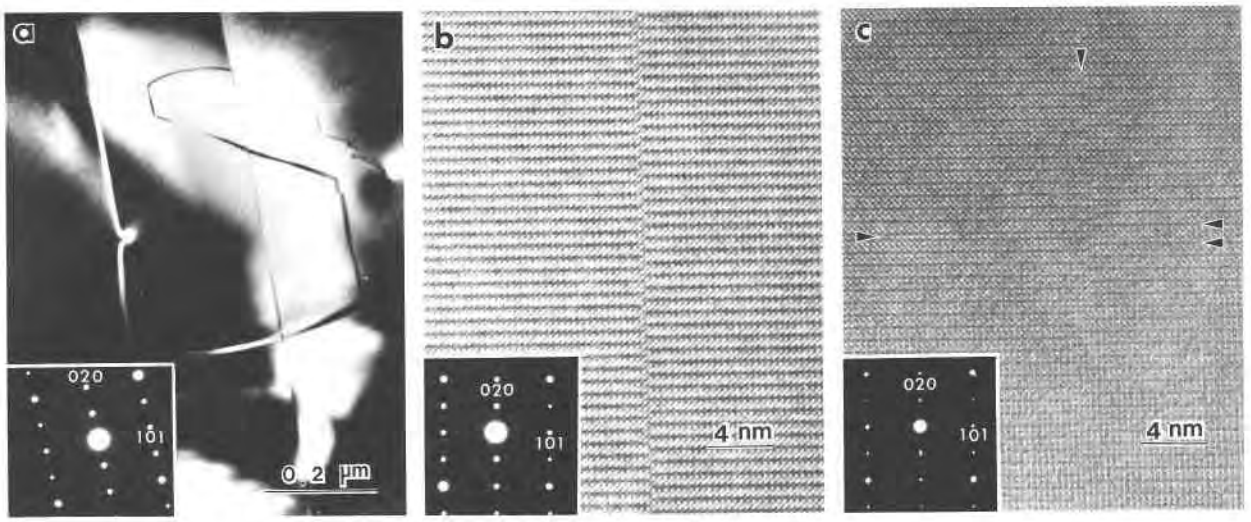

Fig. 15. "Dysanalite" from Kaiserstuhl. (**a**) Curved ½[010] APB crossing a (101) twin. Notice a preferential alignment parallel to (101) that is conservative. (**b**), (**c**) Details of atomic resolution phase contrast micrographs with APBs. (**b**) Conservative APB. (**c**) Nonconservative APB (horizontal) crossing a conservative APB (vertical). Notice that the phase contrast suggests a chemical fault for the nonconservative APB with one fringe on the left side (arrow) and three fringes on the right side (double arrow).

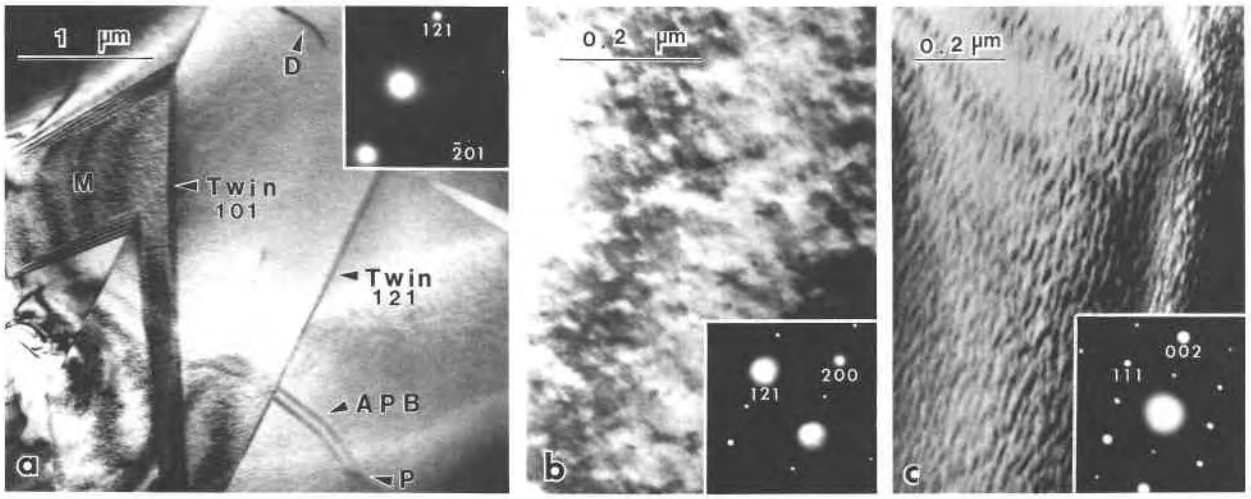

Fig. 17. Mottled contrast, dark-field images. (**a**) General view of complex microstructures in perovskite from Vuore Yavry with {121} and {101} twins, APB, a partial dislocation (P), and a unit dislocation (D). In one of the twins the mottled structure is in good contrast (M). (**b**) Mottled structure in Sebel Yavry perovskite viewed in a direction that shows an irregular morphology. (**c**) Mottled structure with a strong directionality in "dysanalite" from Magnet Cove.

ium titanate transforms to a rhombohedral polymorph. Phase transitions are much more uncertain in $CaTiO_3$. There are reports that it transforms at 1000–1260 °C from cubic to tetragonal and at 600 °C from tetragonal to orthorhombic (Galasso, 1969). It is clear that phase transitions occur at much higher temperatures in calcium titanate than in barium titanate. The latter also has a much lower melting point (De Vries and Roy, 1955). Orthorhombic $CaTiO_3$ perovskite may also become noncentric with atomic shifts along **b**, and this would produce inversion boundaries elongated in the [010] direction.

The presence of those defects does not imply that they formed during phase transformations rather than growth. This is particularly true for twins with irregular contact planes (such as in the Lovozero and Kaiserstuhl samples). It is characteristic of growth twins and was previously discussed by Des Cloizeaux (1878) and Baumhauer (1880), who viewed twins as interpenetrating growth twins, and Klein (1884), who attributed them to a phase transformation but was unsuccessful in inverting orthorhombic perovskite during heating. We have heated perovskite from Akhmatov in situ in a 1.5-MeV HVEM to 900 °C but were unable to cause movement of twin boundaries and APBs.

It is significant that all defects are more common in nonstoichiometric perovskites, "dysanalite," knopite, and loparite. Holmquist (1897) noticed that twinning was more prominent in Ce-rich varieties. The same is true of APBs and the modulated structure that we interpret as inversion boundaries. This suggests that substitution of Nb for Ti and Na, Ce for Ca is partially ordered in orthorhombic perovskite, and phase transformations in such nonstoichiometric perovskites are not purely displacive. This would conform with observations in other $CaXO_3$ compounds where a (111) layered ordering of octahedral cations (cryolite) was observed (Brusset et al., 1970; Galasso, 1970; Longo and Ward, 1961), even though we could find no data in the literature on ordering in natural perovskites. Ionic substitutions may also be accompanied by O and possibly cation vacancies (e.g., Galasso et al., 1959). In nonstoichiometric perovskites, defects may be more common and more stable because phase transitions are no longer purely displacive but require diffusion. It has been observed in ferroelectrics that the transition temperature increases with increasing order on octahedral sites (e.g., Groves, 1986; Setter and Cross, 1980).

Also, addition of Nb and Ce to calcium titanate reduces the transformation temperature. It appears unlikely that pure perovskites of metamorphic origin such as those from Akhmatov and San Benito were ever subjected to temperatures greater than 1000 °C and therefore were never cubic, however, "dysanalite" from alkaline igneous rocks may well have undergone phase transformations. For example, the particularly dense APB structures in Lovozero and Kaiserstuhl perovskites are reminiscent of an order phase transition as is the modulated structure. The high density of nonconservative APBs may accommodate nonstoichiometry in a chemically ordered structure (e.g., Fig. 15c).

One type of defect, ½[100] stacking faults, is not related to a phase transformation. As we have noted, the displacement translates O atoms into O positions but brings cations into vacant sites. Such stacking faults are common in ferroelectric materials (e.g., Prisedsky et al., 1985).

In none of the samples investigated could we identify defects that could be attributed to deformation. Dislocations are rare and always associated with stacking faults and APBs.

In conclusion, we wish to emphasize that microstructures in natural perovskite minerals show a great diver-

sity of defects (Table 3), many of them introduced during phase transformations in the course of varied geological histories. The mineral group deserves a more systematic investigation. In the samples analyzed here we have observed the whole range of microstructures that have been described in synthetic ferroelectric perovskites.

Acknowledgments

We are appreciative of A.G. Bulakh, S.E. Haggerty, A. Sinitsyn, and W. Wimmenauer for providing specimens used in this study. Discussions with D.J. Barber and T. Mitchell were most rewarding. We made extensive use of the facilities at the National Center for Electron Microscopy at LBL, Berkeley, and acknowledge financial support through the Education Abroad Program of UC (H.M., D.S. and H.-R.W.), NSF grants EAR-8816577 and EAR-9104605 (H.-R.W.), and IGPP-LANL. H.-R.W. is grateful for the hospitality at CMS, Los Alamos, during leave as a Berndt Matthias scholar and to J. Donovan for assistance with microprobe analyses.

References cited

Amelinckx, S., Van Tendeloo, G., and Van Landuyt, J. (1989) Electron microscopic studies of oxygen ordering phenomena in $YBa_2Cu_3O_{7-\delta}$. In J.L. Moran-Lopez and I.K. Schuller, Eds., Oxygen disorder effects in high-Tc superconductors, p. 9–45. Plenum Press, New York.

Baba-Kishi, K.Z., and Barber, D.J. (1990) Transmission electron microscope studies of phase transitions in single crystals and ceramics of ferroelectric $Pb(Sc_{0.5}Ta_{0.5})O_3$. Journal of Applied Crystallography, 23, 43–54.

Baumhauer, H. (1880) Über den Perowskit. Zeitschrift für Kristallographie, 4, 187–200.

Bednorz, J.G., and Müller, K.A. (1986) Possible high Tc superconductivity in the Ba-La-Cu-O system. Zeitschrift für Physik, B64, 189–193.

Bonstedt, E.M. (1935) Perovskite. Mineralogiya Soiuza, Moscow and Leningrad Academy of Sciences, ser. A, 5, 39.

Bowman, H.L. (1908) On the structure of perovskite from the Burgumer Alp, Pfitschthal, Tyrol. Mineralogical Magazine, 15, 156–176.

Brusset, H., Gillier-Pandraut, H., and Rajaonera, P. (1970) Synthèse d'oxydes ternaires Ca $B^{V}_{0.5}B^{III}_{0.5}O_3$. Comptes Rendus Académie de Sciences, Paris, 271, série C, 810–813.

Bulakh, A.G., and Abakumova, N.B. (1960) The Sebel-Yavr massif of ultrabasic and alkaline rocks and carbonatites. Sovetskaia Geologiia, 5, 47–59.

Bykova, V.S. (1941) Chemical composition of the Lovozero loparite and a method for its analysis. Doklady Academy of Sciences, USSR, 33, 136.

Des Cloizeaux, A.L.O.L. (1858) Mémoire sur l'emploi des propriétés optiques biréfringentes, pour la distinction et la classification des minéraux cristallisés. Annales des Mines, série 5, 14, 339–420.

——— (1878) Briefliche Mittheilung an Prof. G. vom Rath. Neues Jahrbuch für Mineralogie, Geologie und Palaeonthologie, 43, 372–374.

DeVries, R.C., and Roy, R. (1955) Phase equilibria in the system $BaTiO_3$-$CaTiO_3$. Journal of the American Ceramic Society, 38, 142–146.

Doukhan, N., and Doukhan, J.C. (1986) Dislocations in perovskites $BaTiO_3$ and $CaTiO_3$. Physics and Chemistry of Minerals, 13, 403–410.

Galasso, F.S. (1969) Structure, properties and preparation of perovskite-type compounds, 207 p. Pergamon Press, London.

——— (1970) Structure and properties of inorganic solids, 209 p. Pergamon Press, Oxford.

Galasso, F.S., Katz, L., and Ward, R. (1959) Substitution in the octahedrally coordinated cation positions in compounds of the perovskite type. Journal of the American Chemical Society, 81, 820–823.

Goldschmidt, V.M. (1926) Geochemische Verteilungsgesetze der Elemente. VII, VIII. Skrift. Norske Videnskaps Akademi Klasse 1 Matematisk Naturvidenskapelig Klasse, Oslo, 2 and 8.

Groves, P. (1986) The influence of B-site cation order on the phase transition behaviour of antiferroelectric lead indium niobate. Journal de Physique C, Solid State Physics, 19, 5103–5120.

Guyot, F., Madon, M., Peyronneau, J., and Poirier, J.P. (1988) X-ray microanalysis of high-pressure/high-temperature phases synthesized from natural olivine in a diamond anvil cell. Earth and Planetary Science Letters, 90, 52–64.

Haggerty, S.E., Moore, A.E., and Erlank, A.J. (1985) Macrocryst Fe-Ti oxides in olivine melilites from Namaqualand-Bushmanland, South Africa. Contributions to Mineralogy and Petrology, 91, 163–170.

Hauser, O. (1908) Über den sogenannten Dysanalyt von Vogtsburg im Kaiserstuhl. Zeitschrift für Anorganische Chemie, 60, 237–241.

Holmquist, P.J. (1897) Synthetische Studien über die Perovskit- und Pyrochlormineralien. Ph.D. thesis, University of Uppsala, Uppsala, Sweden.

Hu, M.S., and Fong, D. (1982) In situ TEM studies of ferroelectric phase transitions in $Ba_2NaNb_5O_{15}$ and $LiTaO_3$. Acta Physica Sinica, 31, 815–819.

Hu, M.S., Liao, B., and Feng, D. (1982) Theoretical interpretation of black-white contrast at inversion boundaries. In K.H. Kuo and T. Ko, Eds., New trends of electron microscopy in atom resolution, materials science and biology, p. 140–142. Science Press, Beijing.

Jaffe, B., Cook, W.R., and Jaffe, H. (1971) Piezoelectric ceramics, 318 p. Academic Press, New York.

Kay, H.F., and Bailey, P.C. (1957) Structure and properties of $CaTiO_3$. Acta Crystallographica, 10, 219–226.

Kay, H.F., and Vousden, P. (1949) Symmetry changes in barium titanate at low temperatures and their relation to its ferroelectric properties. Philosophical Magazine, 40, 1019–1040.

Klein, C. (1884) Mineralogische Mittheilungen. Neues Jahrbuch für Mineralogie, Geologie und Paläontologie, 1, 235–258.

Knop, A. (1877) Dysanalyt, ein pyrochlorartiges Mineral. Zeitschrift für Kristallographie, 1, 284–296.

Krause, B., Cowley, J.M., and Wheatley, J. (1979) Short-range ordering in $PbMg_{1/3}Nb_{2/3}O_3$. Acta Crystallographica A, 35, 1015–1017.

Liu, L.G. (1975) Post oxide phase of forsterite and enstatite. Geophysical Research Letters, 2, 417–419.

——— (1976) The post-spinel phase of forsterite. Nature, 262, 770–772.

Longo, J., and Ward, R. (1961) Magnetic compounds of hexavalent rhenium with perovskite-type structure. Journal of the American Chemical Society, 83, 2816–2818.

Madon, M., Bell, P.M., Mao, H.K., and Poirier, J.P. (1980) Transmission electron diffraction and microscopy of synthetic high pressure $MgSiO_3$ phase with perovskite structure. Geophysical Research Letters, 7, 629–632.

Meigen, W., and Hügel, E. (1913) Über die chemische Zusammensetzung des Dysanalyts von Vogtsburg im Kaiserstuhl. Zeitschrift für Anorganische Chemie, 82, 242–248.

Moore, A.E. (1981) Unusual perovskite textural relationships in olivine melilites from Namaqualand-Bushmanland, South Africa. Mineralogical Magazine, 44, 147–150.

Muller, O., and Roy, R. (1974) The major ternary structural families, 487 p. Springer-Verlag, Heidelberg.

Murdoch, J. (1951) Perovskite. American Mineralogist, 36, 573–580.

Nefedov, N.K. (1938) Some new rocks of the Lovozero pluton on the Kola-peninsula. Mémoires Société Russe de Minéralogie, série 2, 67, 507.

Pabst, A. (1951) Minerals of the serpentine area in San Benito County, California. Rocks and Minerals, 26, 478–485.

Poirier, J.P., and Guyot, F. (1989) Deformation mechanisms of crystals with perovskite structure. American Geophysical Union Monograph, 45, 119–123.

Prisedsky, V.V., Pan'ko, G.F., and Klimov, V.V. (1985) Linear and planar faults in electron microscopic structures of PZT crystals. Ferroelectrics, 64, 257–273.

Randall, C.A., Barber, D.J., Whatmore, R.W., and Groves, P. (1986) A TEM study of ordering in the perovskite $Pb(Sc_{0.5}Ta_{0.5})O_3$. Journal of Materials Science, 21, 4456–4462.

Randall, C.A., Barber, D.J., and Whatmore, R.W. (1987a) In situ TEM experiments on perovskite-structured ferroelectric relaxor materials. Journal of Microscopy, 145, 275–291.

——— (1987b) Ferroelectric domain configurations in modified-PZT ceramic. Journal of Materials Science, 22, 925–931.

Rose, G. (1839) Beschreibung einiger neuer Mineralien vom Ural. Poggendorff Annalen der Physik und Chemie, 48, 551–572.

Roth, R.S. (1957) Classification of perovskite and other ABO_3-type compounds. Journal of Research National Bureau of Standards, 58, 75–88.
Setter, N., and Cross, L.E. (1980) The role of B-site cation disorder in diffuse phase transition behavior of perovskite ferroelectrics. Journal of Applied Physics, 51, 4356–4360.
Sörensen, H. (1969) Rhythmic igneous layering in peralkaline intrusions. Lithos, 2, 261–283.
Wang, Y., Guyot, F., Yeganeh-Haeri, A., and Liebermann, R.C. (1990) Twinning in $MgSiO_3$ perovskite. Science, 248, 468–471.
Washington, H.S. (1900) Igneous complex of Magnet Cove, Arkansas. Bulletin of the Geological Society of America, 11, 390–416.
Wimmenauer, W. (1963) Beiträge zur Petrographie des Kaiserstuhls. Teil VI: Die Karbonatite, Teil VII: Zur Petrogenese des Kaiserstuhls. Neues Jahrbuch für Mineralogie, 99, 231–276.
Wu, M.K., Ashburn, J.R., Torng, C.J., Hor, P.H., Meng, R.J., Gao, L., Huang, Z.J., Wank, Y.Q., and Chu, C.W. (1987) Superconductivity at 93 K in a new mixed-phase Y-Ba-Cu-O compound system at ambient pressure. Physical Review Letters, 58, 908–910.

Manuscript received March 26, 1991
Manuscript accepted November 13, 1991